



Absolute airborne gravimetry with a cold atom sensor

Yannick Bidel¹ · Nassim Zahzam¹ · Alexandre Bresson¹ · Cédric Blanchard¹ · Malo Cadoret² · Arne V. Olesen³ · René Forsberg³

Received: 16 October 2019 / Accepted: 13 January 2020
© Springer-Verlag GmbH Germany, part of Springer Nature 2020

Abstract

Measuring gravity from an aircraft is essential in geodesy, geophysics and exploration. It fills a gap between satellite techniques which have a low spatial resolution and traditional ground measurements which can only be performed on ground in accessible areas. Today, only relative sensors are available for airborne gravimetry. This is a major drawback because of the calibration and drift estimation procedures which lead to important operational constraints and measurement errors. Here, we report an absolute airborne gravimeter based on atom interferometry. This instrument has been first tested on a motion simulator leading to gravity measurements noise of 0.3 mGal for 75 s filtering time constant. Then, we realized an airborne campaign across Iceland in April 2017. From repeated line and crossing points, we obtain gravity measurements with an estimated error between 1.7 and 3.9 mGal. The airborne measurements have also been compared to upward continued ground gravity data and show differences with a standard deviation ranging from 3.3 to 6.2 mGal and a mean value ranging from -0.7 to -1.9 mGal.

Keywords Gravimeter · Absolute · Airborne · Atom interferometry

1 Introduction

Airborne gravimetry (Forsberg and Olesen 2010) is a powerful tool for regional gravity mapping. It is relatively cheap, can cover large areas in a relatively short time and has good spatial resolution (around 5 km). Airborne gravimetry is especially interesting in the coastal areas where satellite altimetry does not work or over land areas which are difficult to access with terrestrial gravimetry (mountain areas, glaciers, deserts...) (Forsberg et al. 2014; Abdel Zaher et al. 2018; An et al. 2017).

Currently airborne gravity surveys are carried out with relative sensors (Forsberg et al. 2015; Verdun et al. 2019; Jensen et al. 2019; Studinger et al. 2008) which can only measure the variation of gravity and which suffer from drift. For a gravity survey, one needs thus to go regularly to a

reference point where the gravity is known or where a static absolute gravimeter is located. Additionally, the flight path design requires cross-over tracks, which are used in classical airborne gravimetry to determine drift parameters and signal validation. Therefore, the use of a relative gravimeter has important operational constraints which increase the time and the cost of gravimetry surveys.

Two technologies exist for absolute gravimeter: classical and quantum. In classical gravimeters, the acceleration of a free falling corner cube is measured with optical interferometry (Niebauer et al. 1995). These instruments are commercially available and can be operated only in static conditions. For dynamic operation, only one feasibility study done with a modified FGL gravimeter on an aircraft can be found in the literature (Baumann et al. 2012). In a quantum gravimeter, gravity is obtained from the acceleration measurement of a gas of cold atoms using matter wave interferometry (Peters et al. 2001). This latest technology has now reached the performance of optical gravimeter (Gillot et al. 2014; Freier et al. 2016; Hu et al. 2013) and start to be commercialized (Ménoret et al. 2018). Moreover quantum technology seems more adapted to dynamic environments because there is no mechanical moving parts and the repetition rate is higher. Recently, absolute ship borne gravimetry

✉ Yannick Bidel
yannick.bidel@onera.fr

¹ DPHY, ONERA, Université Paris Saclay, 91123 Palaiseau, France

² LCM-CNAM, 61 Rue du Landy, 93210 La Plaine Saint-Denis, France

³ Geodynamics Department, National Space Institute, DTU Space, Kongens Lyngby 2800, Denmark

with sub-mGal precision has been reported using a quantum gravimeter (Bidel et al. 2018). The precision of the quantum gravimeter called GIRAFE has been compared to a commercial spring gravimeter and showed better performances during the marine gravity campaign.

Here, we report absolute airborne gravimetry with the GIRAFE atom gravimeter previously tested on a ship. In the first part, the atom gravimeter will be shortly described and the modifications compared to the previous marine test will be reported. In the second part, the airborne gravity campaign done in Iceland will be described. In the third part, the data processing to estimate gravity disturbance will be explained. Then, the results of the airborne campaign will be shown. Finally, the airborne measurements will be compared with ground data.

2 Cold atom gravimeter

2.1 Apparatus description

The description of the gravimeter can be found in the reference (Bidel et al. 2018) and we provide here only a short description. The gravimeter is composed of an atom sensor which provides an absolute measurement of the acceleration, a gyro-stabilized platform which maintains the accelerometer aligned with the local gravity acceleration despite angular movements of the carrier and systems which provide the lasers and microwaves needed to the atom sensor and perform data acquisition and processing.

The principle of the atom accelerometer is based on the acceleration measurement of a free falling test mass. The test mass is a gas of cold Rubidium 87 atoms produced by laser cooling and trapping method. The trapped gas contains typically 10^6 atoms and has a size of 1 mm and a temperature of $1 \mu\text{K}$. After release from the trap, atoms are let in free fall and their accelerations are measured by atom interferometry. For that, the atoms are submitted to three laser pulses separated by a duration T . The laser pulses drive two photon Raman transitions between the two hyperfine ground states of the atoms ($F = 1$ and $F = 2$) and give a momentum to the atoms when they undergo the transition. The first pulse acts as a matter wave beam splitter, the second one acts as a mirror and the last one recombines the matter waves (see Fig. 1). The signal of the atom interferometer is then obtained by measuring the proportion of atoms in the two hyperfine states by laser-induced fluorescence method. The output P of the atom sensor is proportional to the cosine of the acceleration with a period equal to $\lambda/(2T^2)$ where $\lambda = 780 \text{ nm}$ is the laser wavelength. In our sensor the pulse separation T can be changed. Our 14 mm falling distance allows us to change T from 0 to 20 ms. For $T = 20 \text{ ms}$, the acceleration period is equal to 10^{-3} m s^{-2} and is small compared to typical varia-

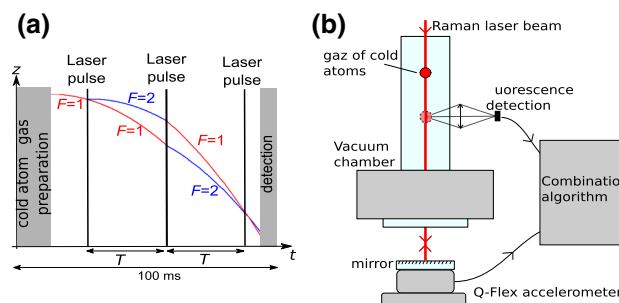


Fig. 1 Principle of the atom accelerometer. **a** Temporal sequence ($F = 2$ and $F = 1$ are the two hyperfine ground states of Rubidium 87 atoms). **b** Set-up of the atom accelerometer

tions of acceleration in a moving vehicle. There is, therefore, an ambiguity to determine the acceleration from the measurement of the atom sensor. Many values of acceleration are possible for a given value of the output of the atom sensor. To overcome this limitation, we combine the atom sensor with a classical accelerometer. We use a Qflex force balanced accelerometer from Honeywell but other low noise classical accelerometers could work also. The classical accelerometer is used to give a first rough estimation of the acceleration in order to determine which value of acceleration corresponds to the signal of the atom sensor. The classical accelerometer is also used to measure the acceleration during the measurement dead times of the atom sensor which occur during the cold atoms preparation and during the detection. On the other hand, the atom accelerometer allows to estimate the bias of the classical accelerometer and thus improving its precision.

This hybridization is working if the difference of acceleration given by the two sensors is much smaller than the atom accelerometer signal period ($\lambda/(2T^2)$). Different limitations can induce differences of acceleration and specially in hard dynamical environments (transfer function uncertainties, alignment defaults, measurement points non-co-located). In order to be always operational, the gravimeter algorithm is changing automatically the atom interrogation time T ($T = 2.5, 5, 10$ or 20 ms) by comparing the rms on the difference of acceleration given by the two sensors and the atom accelerometer period. If the rms difference is small, the algorithm will increase the interrogation time and the gravimeter will thus access to better precision due to the scale factor increase. If the rms difference is too big, the algorithm will decrease the interrogation time T which will allow the gravimeter to keep working, but this will also decrease the precision measurement. During the different tests described in this article, the interrogation time will stay at $T = 20 \text{ ms}$ excepted during turbulent parts of flights where the interrogation time switches to $T = 10 \text{ ms}$.

This atom accelerometer has been implemented in a compact housing consisting of a cylinder of 22 cm diameter and 52 cm height. It is composed of a vacuum chamber made

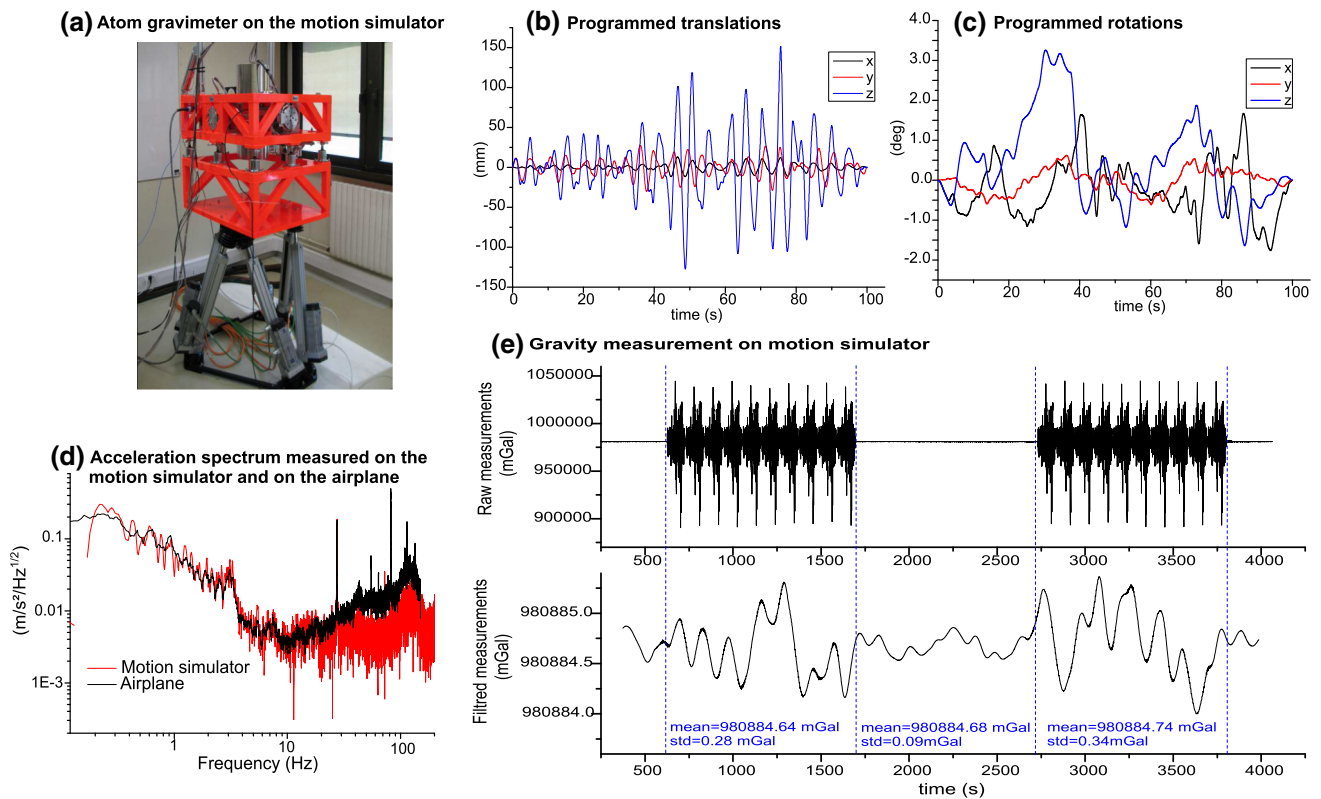


Fig. 2 Test on a motion simulator. **a** Picture of the atom gravimeter on the motion simulator. **b** Programmed translation on the motion simulator along the three axes. **c** Programmed rotation on the motion simulator along the three axes. **d** Vertical acceleration spectrum measured on the

motion simulator (red) and on the real flight (black). **e** Gravity measurement on the motion simulator (top: raw data, bottom, filtered data with fourth-order Bessel filter of time constant 75 s)

of glass in which the atoms are produced and interrogated, magnetic coils, optics for shaping all the laser beams and collecting the fluorescence of the atoms, two layers of mu-metal for shielding the external magnetic field and classical accelerometers. This sensor is integrated in a two axes stabilized gimbaled platform made by IMAR. The platform is stabilized using an integrated inertial measurement system and maintains the sensor head aligned with the gravity acceleration with a precision of 0.1 mrad. The platform is mounted on passive vibration isolators which have a resonant frequency of 12 Hz.

In static condition, the sensitivity of the gravimeter is equal to $0.8 \text{ mGal Hz}^{-1/2}$ and the accuracy is estimated at 0.17 mGal for $T = 20 \text{ ms}$ (Bidel et al. 2018).

2.2 Improvement of the force balanced accelerometer model for high-frequency vibrations

In airborne environment, the gravimeter is subjected to strong vibrations. In this case, if we do not take into account the exact frequency transfer function of the force balanced accelero-

meter, the acceleration given by the atom and the force balanced accelerometer could be different and not negligible compared to the period of the atom accelerometer signal (10^{-3} m s^{-2} for $T = 20 \text{ ms}$). In this situation, the hybridization method will not work properly and will lead to decrease in performance of the gravimeter. The transfer function of the force balanced accelerometer has thus to be known precisely and compensated in order to optimize the precision of our instrument.

The transfer function of our force balanced accelerometer (Qflex) has been estimated empirically by minimizing the difference between the acceleration from the force balanced accelerometer and the atom accelerometer in the presence of high-frequency vibrations. For that, we model the transfer function of the force balanced accelerometer by a first-order damped harmonic oscillator:

$$h_{\text{FB}}(s) = \frac{\omega_0^2}{s^2 + \Gamma s + \omega_0^2}; \quad s = j\omega \tag{1}$$

where $j^2 = -1$, ω is the angular frequency, ω_0 is the resonant angular frequency and Γ is the damping rate. Minimizing the

difference between atom and forced balanced accelerometer lead to $\omega_0 = 1.57 \times 10^3 \text{ s}^{-1}$ and $\Gamma = 2.42 \times 10^3 \text{ s}^{-1}$.

2.3 Test on a motion simulator

The atom gravimeter has been tested on a motion simulator reproducing as well as possible the motion of an aircraft (see Fig. 2a). For that, we took 100 s of IMU data coming from a DTU flight campaign in Antarctica with a Twin Otter (non-turbulent part). Then we programmed the motion simulator to reproduce the three translations and three rotations measured by the IMU. The translations were high pass filtered at a frequency of 0.2 Hz for having translations in the range of the motion simulator ($\pm 0.18\text{m}$).

To check the fidelity of the simulation, we measured the vertical acceleration on the base plate of the gravimeter and we compared it with the acceleration coming from the IMU of the plane. We notice that the motion simulator reproduced well the acceleration spectrum between 0.2 and 20 Hz (see Fig. 2d).

The gravimeter was subjected to a simulated airborne environment during two periods of 1000 s with a break of 1000 s between them (see Fig. 2e). The gravimeter measurement was low pass filtered by a fourth-order Bessel filter of 75 s time constant (see Sect. 4.3). We notice that the mean value of measured gravity has not significantly changed during the period of motion simulation. The rms noise on the filtered gravity measurements is equal to 0.3 mGal during motion and 0.1 mGal during static period.

3 Airborne gravity campaign in Iceland

The campaign took place across Iceland, using a Twin Otter DHC-6 from Norlandair (Akureyri) and consisted of repeat flights in northern Iceland and a small demonstration survey pattern over the Vatnajökull (see Fig. 3).

Before airborne tests, we performed static measurement in the plane hangar. We obtained a gravity measurement of $g = 982337.37 \pm 0.17 \text{ mGal}$ at 99 cm above the ground which agrees with a previous measurement made with a A10 absolute gravimeter to within 0.1 mGal.

The atom gravimeter was tested during four flights: the first one was a straight line back and forth between Akureyri and Snæfellsjökull. The goal of this flight is to evaluate the reproducibility of the gravity measurement. The last three measurement flights were above Vatnajökull. The goal was here to make a gravity model of the area. The duration of each flight was 3–4 h. The vertical acceleration measured during the flights is given in Fig. 3. The acceleration level during the flights is not homogeneous. During turbulent part, one can have acceleration variations up to 10 m s^{-2} and during quiet part below 0.3 m s^{-2} . Most of the time the level of

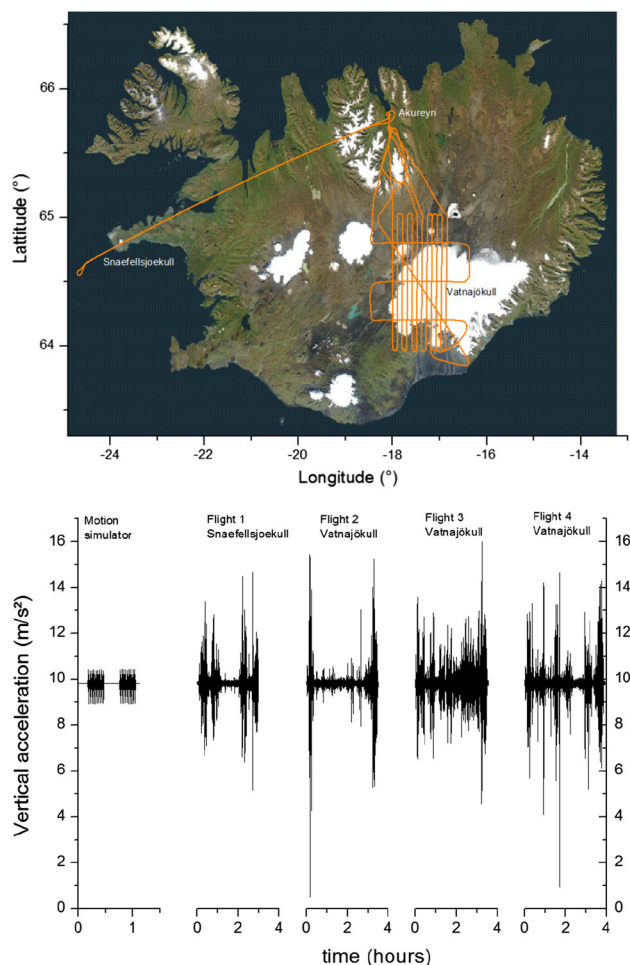


Fig. 3 Top: Flight plan of Iceland gravity campaign. Bottom: Raw vertical acceleration undergone by the atom gravimeter during the motion simulator test and during flights in Iceland. The acceleration has been measured in the sensor head at a rate of 10 Hz

acceleration is larger than the one we simulated on the motion simulator.

4 Data processing and gravity estimation

4.1 Kinematic acceleration and Eötvös effect

The gravimeter is not only measuring the gravity acceleration but also the kinematic acceleration of the plane and the acceleration due to the coupling to Earth rotation (Eötvös effect). The acceleration measured by the gravimeter is equal to:

$$a_{\text{meas}} = g + \ddot{h} + a_{\text{Eöt}} \quad (2)$$

where g is the gravity acceleration (g is positive when downward), \ddot{h} is the time second derivative of h the ellipsoidal height (h is positive when upward) and represents the ver-

tical kinematic acceleration of the plane, $a_{E\ddot{o}t}$ is the Eötvös acceleration which is equal to:

$$a_{E\ddot{o}t} = -2 \omega_E \cdot \cos(\varphi) \cdot v_E - \frac{v_E^2}{N(\varphi) + h} - \frac{v_N^2}{M(\varphi) + h} \quad (3)$$

with:

$\omega_E = 7.292115 \cdot 10^{-5} \text{ s}^{-1}$: Earth’s rotation rate (inertial frame);

φ : Latitude;

v_E : East velocity;

v_N : North velocity;

h : Altitude;

$M(\varphi) = \frac{a^2 \cdot b^2}{(a^2 \cos(\varphi)^2 + b^2 \sin(\varphi)^2)^{3/2}}$: Earth’s radius of curvature in the (north-south) meridian;

$N(\varphi) = \frac{a^2}{(a^2 \cos(\varphi)^2 + b^2 \sin(\varphi)^2)^{1/2}}$: Earth’s radius of curvature in the prime vertical;

$a = 6378137.0 \text{ m}$: Earth’s equatorial radius (WGS84);

$b = 6356752.3 \text{ m}$: Earth’s polar radius (WGS84).

The vertical kinematic acceleration and Eötvös effect are calculated with GNSS data (φ : latitude, λ : longitude, h : altitude) at 10 Hz ($dt = 0.1 \text{ s}$) based on differential and post-post-processed DGPS data. The level arm between the GNSS antenna and the gravimeter has been taken into account. The vertical kinematic acceleration, the east velocity and the north velocity have been calculated using the following equations:

$$\begin{aligned} \ddot{h}(t) &= \frac{-2h(t) + h(t + dt) + h(t - dt)}{dt^2} \\ v_E(t) &= \frac{\lambda(t + dt) - \lambda(t - dt)}{2 dt} \cdot (N(\varphi) + h) \cdot \cos(\varphi) \\ v_N(t) &= \frac{\varphi(t + dt) - \varphi(t - dt)}{2 dt} \cdot (M(\varphi) + h) \end{aligned} \quad (4)$$

4.2 Missing data points and interpolation

The gravimeter provides acceleration measurements at a rate of 10 Hz. The precise timing of the measurements compared to the GNSS is crucial in order to correct precisely from the effect of kinematic acceleration and Eötvös effect which can be up to 10^6 times bigger than the gravity disturbance signal. However, the timing of the gravimeter measurements is not precise and has the following default:

- The clock of the computer which controls the gravimeter is not precise (relative drift of 3×10^{-5}) and has an unknown delay compared to the GNSS time base;

- The recording time has jitters compared to the real measurement time of the gravimeter;
- There are missing data points (typically 1 per hour);
- There is a 20ms offset of the effective measurement time compared to the recording measurement time when the interrogation time T of the gravimeter is changing between 10 and 20 ms.

We try to correct these limitations by using the following procedure. First, the missing data points are filled by inserting extrapolated measurements. Second, we assume that the measurement times of the gravimeter are given by: $t_i = i \cdot dt + T + t_0$ where $dt \sim 0.1 \text{ s}$ is the time interval between measurements and T is the interrogation time used by the gravimeter. Then, we adjust the parameter dt and t_0 in order that the acceleration given by the GNSS and the gravimeter match at the beginning and at the end of the acquisition period.

4.3 Lowpass filtering

The gravimeter measurement, the kinematic acceleration and the Eötvös effect are filtered with a fourth-order Bessel low pass filter of time constant $\tau = 130\text{s}$:

$$h(s) = \frac{105}{s^4 + 10s^3 + 45s^2 + 105s + 105}; \quad s = j\omega\tau \quad (5)$$

For a plane of velocity v , this gives a spatial resolution equal to $\approx 1.035 \cdot v \cdot \tau$. The spatial resolution is here defined as the FWHM of the signal obtained with a Dirac input signal. For the filter to work properly, we linearly extrapolate the gravity measurements points and the GNSS data on a regular time base at 10 Hz. The filter time constant has been increased for airborne tests compared to motion simulator tests ($\tau = 75\text{s}$) because the level of acceleration is larger (see Fig. 3).

4.4 Gravity disturbance calculation

The gravity disturbance is obtained by subtracting the gravity measurements by the WGS84 normal gravity model taking into account altitude and latitude effects (Torge 1989):

$$g_0 = \frac{a \cdot g_E \cdot \cos(\varphi)^2 + b \cdot g_P \cdot \sin(\varphi)^2}{\sqrt{a^2 \cdot \cos(\varphi)^2 + b^2 \cdot \sin(\varphi)^2}} \cdot (1 + \gamma_1 \cdot h + \gamma_2 \cdot h^2) \quad (6)$$

with:

$$g_E = 9.7803253359 \text{ ms}^{-2} \quad (\text{WGS84})$$

$$g_P = 9.8321849378 \text{ ms}^{-2} \quad (\text{WGS84})$$

Table 1 Error from platform misalignment

	$\delta g_{\text{tilt max}}$
Flight 1: Akureyri–Snæfellsjökull	1 mGal
Flight 2: Vatnajökull	20 mGal
Flight 3: Vatnajökull	4 mGal
Flight 4: Vatnajökull	5 mGal

$$\gamma_1 = -\frac{2}{a} \left(1 + f + \frac{a^2 \cdot b \cdot \omega_E^2}{G \cdot M} - 2 \cdot f \cdot \sin(\varphi)^2 \right)$$

$$\gamma_2 = \frac{3}{a^2}$$

$$f = \frac{a - b}{a}$$

$$G \cdot M = 3.986004418 \cdot 10^{14} \text{ m}^3 \cdot \text{s}^{-3} \text{ (WGS84)}$$

$$a = 6378137.0 \text{ m : Earth's equatorial radius (WGS84)}$$

$$b = 6356752.3 \text{ m : Earth's polar radius (WGS84)} \quad (7)$$

4.5 Correction of the alignment errors of the platform

Alignment errors of the platform make the gravimeter less sensitive to vertical gravity acceleration and make it sensitive to horizontal accelerations. To evaluate this error, we follow the modeling approach described in the thesis of Olesen (2002). The error on gravity measurements caused by a platform misalignment is given by:

$$\delta g_{\text{tilt}} = \frac{\phi_x^2 + \phi_y^2}{2} \cdot g + \phi_x \cdot a_x + \phi_y \cdot a_y \quad (8)$$

where ϕ_x and ϕ_y are the misalignment angles compared to the direction of the gravity acceleration and a_x and a_y are the horizontal accelerations. In this expression, we assume that the misalignment angles are small ($\phi_x, \phi_y \ll 1$, the angles are here expressed in rad). The misalignment angles are estimated by comparing the accelerations measured by horizontal force balance accelerometers located in the sensor head and the kinematic acceleration deduced from GNSS data:

$$\phi_{x(y)} = \frac{a_{x(y)} - a_{x(y)\text{GNSS}}}{g} \quad (9)$$

The parameters $a_x, a_y, a_{x\text{GNSS}}$ and $a_{y\text{GNSS}}$ have been pre-filtered by a fourth-order Bessel filter of time constant 40 s. The correction tilt δg_{tilt} obtained has been filtered with the same filter as the gravimeter measurement, i.e., a fourth-order

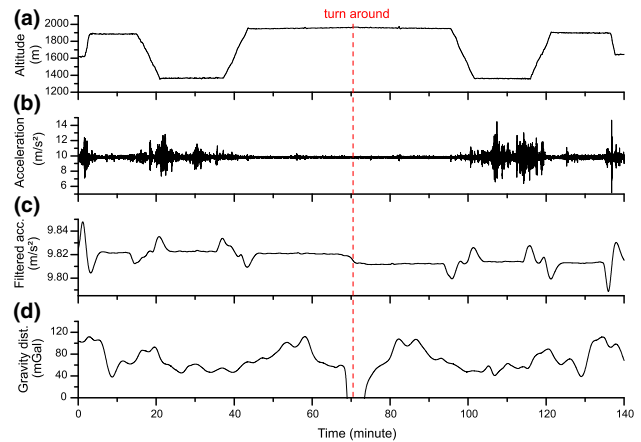


Fig. 4 Gravity measurements on the Akureyri Snæfellsjökull line. **a** Altitude of the plane. **b** Raw acceleration measured by the gravimeter. **c** Filtered acceleration measured by the gravimeter (fourth-order low pass Bessel filter of time constant 130 s). **d** Estimated gravity disturbance with the 130 s low pass filter

Bessel filter with a time constant of 130 s. We obtained alignment errors up to 20 mGal in period of gravity measurements, i.e., constant yaw. This error is very different from flight to flight (see Table 1).

5 Airborne test results

5.1 Akureyri–Snæfellsjökull

The airborne measurements obtained on the line Akureyri–Snæfellsjökull flown back and forth are given in Fig. 4. The plane was flying at two elevations (1900 m and 1400 m) in order to be as close as possible to the ground and thus to the gravity sources. The 1900 m altitude corresponds to a mountain area and the 1400 m elevation corresponds to a plain area. The velocity of the plane was 76 m/s. With the fourth-order Bessel filter of time constant 130 s, one obtains a spatial resolution of 10.5 km (FWHM). On the filtered acceleration graph, one can see clearly the Eötvös effect when the plane turned around. Indeed, at this point the velocity changes sign and the Eötvös acceleration also. One can also see clearly the effect of the vertical acceleration of the plane at the moment where the plane was changing of elevation. In order to estimate the repeatability of the measurements, we compared the gravity measured forward and backward (see Fig. 5). The difference between forward and backward has a mean of 0.6 mGal and a standard deviation of 5.5 mGal. One notices that the big difference in the center corresponds to some missing measurement points on the gravimeter measurements. If one restricts to the area where there is no missing points, one obtains a standard deviation of 3.4 mGal close to Snæfellsjökull and 2.4 mGal close

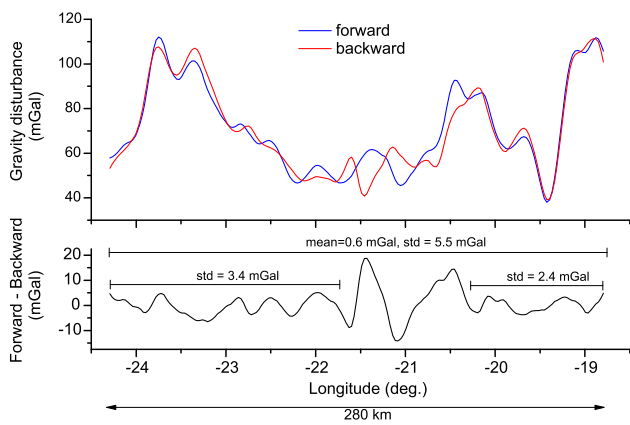


Fig. 5 Comparison of the gravity measurement along the line Akureyri-Snaefellsjökull for the forward and backward flight

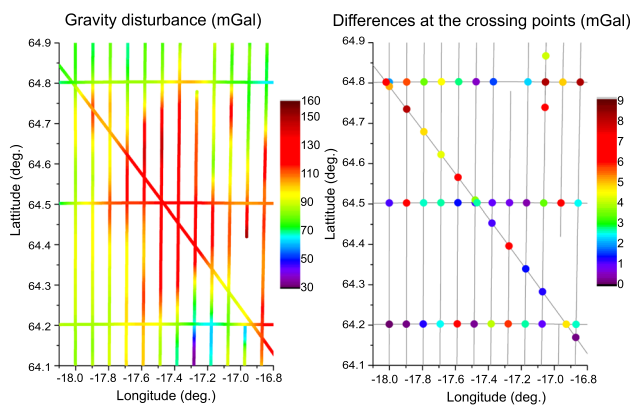


Fig. 6 Vatnajökull gravity measurements. Left: gravity disturbance. Right: Crossing points differences

to Akureyri. Assuming uncorrelated errors between forward and backward measurements, the measurement error is given by the standard deviation of the difference divided by $\sqrt{2}$. One obtains thus an estimated error ranging from 1.7 to 3.9 mGal depending on the area considered.

5.2 Vatnajökull

During three flights, we measured gravity above the area of Vatnajökull ice cap along 16 lines. The altitude of the plane was 2600 m and its velocity 76 m/s. We use the same filter than before leading to a spatial resolution of 10.5 km. The gravity disturbance measurements obtained are reported in Fig. 6. One notices two measurements area missing which correspond to moments where the gravimeter was not operational due to laser misalignment problems. The difference at the crossing points is ranging from 0 to 8 mGal with a rms value of 3.9 mGal. Assuming no correlation, one can estimate a measurement error of 2.8 mGal (rms value divided by $\sqrt{2}$).

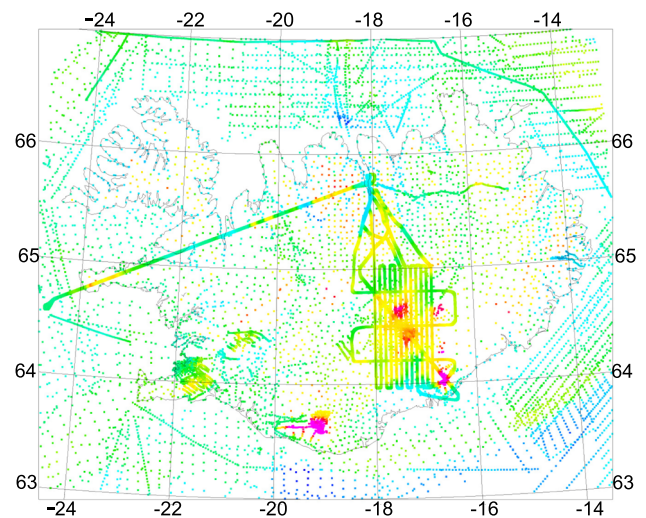


Fig. 7 Iceland gravity coverage (ground measurements), overlaid with the cold atom gravimetry results. The positive free-air anomalies shown are predominantly due to volcanoes under the ice caps, and topographic highs

6 Comparison with ground data

The Iceland region has a relatively dense ground gravity coverage, as shown in Fig. 7. The use of upward continued surface gravimetry represents an independent validation opportunity for the cold atoms gravimetry results. The Iceland gravity data were surveyed primarily in the 1980's, and provided by Landmælingar Islands (Iceland Geodetic Survey).

The upward continuation estimation of the free-air anomalies at altitude was done using the GRAVSOFT suite of programs (Tscherning et al. 1992), using standard remove-restore techniques of physical geodesy [use of EGM2008 as reference field, integration of terrain effects by prism integration, and upward continuation to the flight altitude by fast Fourier transform methods (Schwarz et al. 1990)]. A digital terrain model at 200 m resolution was used and combined with a ice cap thickness model of the 3 main ice caps in Iceland (including Vatnajökull), derived from radar echo sounding and also provided by Landmælingar Islands, as part of cooperation on geoid determination.

The predicted versus the observed cold atom gravimetry results are shown in Figs. 8 and 9, with the predicted data at altitude filtered with a similar fourth-order Bessel filter with time constant 130 s, to match the airborne data filter. One notices that similar gravity signals are obtained with the two models confirming the relevance of the cold atom gravimeter measurements. For the line Akureyri-Snaefellsjökull, we obtained a standard deviation on the difference equal to 4.0 mGal and a mean difference of -1.9 mGal; it should be noted that some part of this line was over fjords with no surface gravity, and the upward continued gravity data may therefore

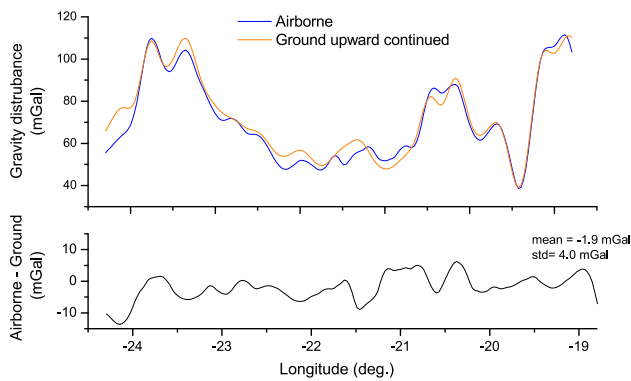


Fig. 8 Comparison between airborne measurements (average of forward and backward) and ground measurements upward continued along the line Akureyri–Snæfellsjökull

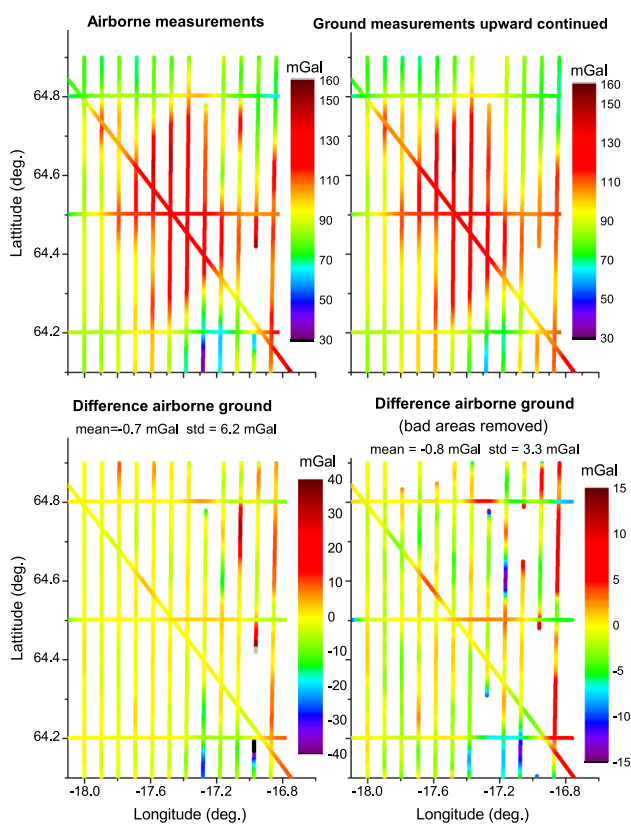


Fig. 9 Comparison between airborne measurements and ground measurements upward continued over Vatnajökull

be biased. For Vatnajökull flights, we obtained a standard deviation on the difference equal to 6.2 mGal and a mean difference of -0.7 mGal. We noticed that in some areas (see Fig. 9), the difference between airborne and ground is large. These areas correspond to the beginning of a track (after a plane turn), to a period around laser misalignment problem and to a severe turbulence period ($\varphi = 64.7^\circ$, $\lambda = -17.1^\circ$). If we removed these areas, the standard deviation becomes

two times smaller (3.3 mGal) and the mean difference is approximately the same (-0.8 mGal).

An issue for the comparison of surface and airborne data is also the possible geodynamic gravity changes between the surface and airborne gravity epochs, since several volcanic eruptions have taken place, especially the Bardarbunga eruption of 2014, which had major dyke intrusion activity in the northwestern region of the Vatnajökull ice cap.

7 Conclusion

In conclusion, we demonstrated for the first time airborne gravity measurements and survey with an atom interferometry sensor. The main advantage of this technology is that it provides absolute measurements (no drift and no calibration needed). The precision of the gravity measurements has been estimated thanks to comparison on a forward and backward line and to differences at crossing points. Measurement errors ranging from 1.7 to 3.9 mGal have been obtained. The airborne gravity measurements have been also compared to upward continued ground truth. The standard deviation on the difference is ranging from 3.3 to 6.2 mGal, and the mean value on the difference is ranging from -0.7 to -1.9 mGal.

This is a promising result for a sensor which was designed for marine application. The precisions obtained here could be improved by optimizing the instrument on the followings points. First, the measurement timing of the atom gravimeter could be improved by having measurements points on a regular time basis (GNSS dating). Then, the missing measurement points have to be suppressed. Finally, the gyro-stabilized platform and the hybridization algorithm between the classical and the atom accelerometer should be optimized for airborne environment. With these improvements which are not inherent to atom interferometry technology, atom gravimeter should reach the state of the art with sub-mGal precision on airborne survey with still absolute measurements.

Finally, these results show the maturity of cold atom technology for onboard application and support the development of atom interferometry sensor for measuring the Earth gravity field from space (Carraz et al. 2014; Abrykosov et al. 2019).

Acknowledgements The development of the atom gravimeter was funded by the French Defense Agency (DGA). The Iceland GIRAFE cold atom airborne campaign was carried out with support from ESA (Cryovex), ONERA and DTU Space. Nordlandair, Iceland, provided excellent support for the challenging installation of the complex system in the Twin Otter TF-POF. We thank Landmælingar Islands for providing the permission at short notice for the test campaign in Iceland.

Author contributions YB, NZ, AB, CB and MC designed, built and tested the atom gravimeter. YB, NZ, AB, AVO and RF participated to the

Iceland gravity campaign. Data processing and ground comparison were done by YB, AVO and RF, YB wrote the manuscript with contributions from all authors.

Data Availability Statement The data used in this manuscript are available from the corresponding author upon request.

References

- Abdel Zaher M, Saibi H, Mansour K, Khalil A, Soliman M (2018) Geothermal exploration using airborne gravity and magnetic data at Siwa Oasis, Western Desert, Egypt. *Renew Sustain Energy Rev* 82:3824–3832
- Abrykosov P, Pail R, Gruber T, Zahzam N, Bresson A, Hardy E, Christophe B, Bidel Y, Carraz O, Siemes C (2019) Impact of a novel hybrid accelerometer on satellite gravimetry performance. *Adv Space Res* 63(10):3235–3248
- An L, Rignot E, Elieff S, Morlighem M, Millan R, Mouginit J, Holland DM, Holland D, Paden J (2017) Bed elevation of Jakobshavn Isbræ, West Greenland, from high-resolution airborne gravity and other data. *Geophys Res Lett* 44(8):3728–3736
- Baumann H, Klingelée EE, Marson I (2012) Absolute airborne gravimetry: a feasibility study. *Geophys Prospect* 60(2):361–372
- Bidel Y, Zahzam N, Blanchard C, Bonnin A, Cadoret M, Bresson A, Rouxel D, Lequentrec-Lalancette MF (2018) Absolute marine gravimetry with matter-wave interferometry. *Nat Commun* 9:627
- Carraz O, Siemes C, Massotti L, Haagmans R, Silvestrin P (2014) A spaceborne gravity gradiometer concept based on cold atom interferometers for measuring Earth's gravity field. *Microgravity Sci Technol* 26(3):139–145
- Forsberg R, Olesen AV (2010) Airborne gravity field determination. *Sciences of geodesy-I: advances and future directions*. Springer, Berlin, pp 83–104
- Forsberg R, Olesen AV, Einarsson I, Manandhar N, Shreshta K (2014) Geoid of nepal from airborne gravity survey. *Int Assoc Geod Symp* 139:521–527
- Forsberg R, Olesen AV, Einarsson I (2015) Airborne gravimetry for geoid determination with lacoste romberg and chekan gravimeters. *Gyrosc Navig* 6(4):265–270
- Freier C, Hauth M, Schkolnik V, Leykauf B, Schilling M, Wziontek H, Scherneck H, Müller J, Peters A (2016) Mobile quantum gravity sensor with unprecedented stability. In: *Journal of Physics: Conference Series*, vol 723
- Gillot P, Francis O, Landragin A, Pereira Dos Santos F, Merlet S (2014) Stability comparison of two absolute gravimeters: optical versus atomic interferometers. *Metrologia* 51(5):L15
- Hu Z-K, Sun B-L, Duan X-C, Zhou M-K, Chen L-L, Zhan S, Zhang Q-Z, Luo J (2013) Demonstration of an ultrahigh-sensitivity atom-interferometry absolute gravimeter. *Phys Rev A* 88:043610
- Jensen TE, Nielsen JE, Olesen AV, Forsberg R (2019) Strapdown airborne gravimetry using a combination of commercial software and stable-platform gravity estimates. *International association of geodesy symposia*, vol 148. Springer, New York, pp 103–109
- Ménoret V, Vermeulen P, Le Moigne N, Bonvalot S, Bouyer P, Landragin A, Desruelle B (2018) Gravity measurements below 10⁻⁹ g with a transportable absolute quantum gravimeter. *Sci Rep* 8(1):12300
- Niebauer TM, Sasagawa GS, Faller JE, Hilt R, Klopping F (1995) A new generation of absolute gravimeters. *Metrologia* 32(3):159–180
- Olesen AV (2002) Improved airborne scalar gravimetry for regional gravity field mapping and geoid determination. PhD thesis, University of Copenhagen
- Peters A, Chung KY, Chu S (2001) High-precision gravity measurements using atom interferometry. *Metrologia* 38(1):25–61
- Schwarz KP, Sideris MG, Forsberg R (1990) The use of fft techniques in physical geodesy. *Geophys J Int* 100(3):485–514
- Studinger M, Bell R, Frearson N (2008) Comparison of airgrav and gt-1a airborne gravimeters for research applications. *Geophysics* 73(6):I51–I61
- Torge W (1989) *Gravimetry*. W. de Gruyters, New York
- Tscherning CC, Forsberg R, Knudsen P (1992) The gravsoft package for geoid determination. In: *Proceedings of IAG first continental workshop for the geoid in Europe, Prague*, pp 327–337
- Verdun J, Bayer R, Klingelée EE, Cocard M, Geiger A, Halliday ME (2019) Airborne gravity measurements over mountainous areas by using a lacoste and romberg air-sea gravity meter. *Geophysics* 67(3):807–816